RSC Advances

ROYAL SOCIETY OF CHEMISTRY

www.rsc.org/advances

Reduced efficiency roll-off in phosphorescent OLEDs with a stack emitting layer facilitating triplet exciton diffusion

Shuqing Yuan[a], Yuying Hao[a*], Yanqin Miao[b], Qinjun Sun[a], Zhanfeng Li[a], Yanxia Cui[a], Hua Wang[b], Fang Shi[a], Bingshe Xu[b]

[a]*Key Lab of Advanced Transducers and Intelligent Control System of Ministry of Education, College of Physics and Optoelectronics, Taiyuan University of Technology, Taiyuan 030024, China*

[b]*Key Laboratory of Interface Science and Engineering in Advanced Materials, Taiyuan University of Technology, Taiyuan 030024, China*

[*]Correspondence author: haoyuyinghyy@sina.com

Abstract

A high efficiency and low efficiency roll-off phosphorescent organic light-emitting diode (PHOLED) is demonstrated based on a stacked emissive layer by alternating [CBP:4 wt% $Ir(ppy)_3$ (5 nm)] and [CBP:8 wt% $Ir(ppy)_3$ (5 nm)] ultrathin films. The results show that when the number of the stack cell is equal to three, the peak current efficiency of *ca.* 48.8 cd/A and the peak external quantum efficiency (EQE) of *ca.* 19.6% are obtained and kept until 1000 cd/m^2. As the luminance further increases from 1000 to 100000 cd/m^2, there only exists a less than 25.1% drop in current efficiency and 25.5% drop in EQE. The improved properties for the proposed PHOLED are attributed to greatly weakened triplet exciton quenching due to the very effective triplet exciton diffusion by the abovementioned stacked emissive structure.

Keywords: Phosphorescent organic light-emitting diodes (PHOLEDs); Efficiency roll-off; Stacked emissive layer; Triplet exciton diffusion

1. Introduction

Phosphorescent organic light-emitting diodes (PHOLEDs) have attracted extensive attention due to their potentially high quantum efficiency by harvesting both the singlet and triplet excitons.[1-5] However, PHOLEDs often suffer from the efficiency roll-off at high current density, [6-8] which is very detrimental for high-brightness lighting applications. The main reason for the efficiency roll-off is the non-radiative triplet exciton quenching including triplet-triplet exciton annihilation (TTA) and triplet-polaron annihilation (TPA) in the emissive layer (EML).[9, 10] To suppress triplet exciton quenching, on one hand, the charge carrier in device should be as balanced as possible to minimize polaron accumulation at the interface.[11-13] On the other hand, the local triplet exciton density should be decreased by extending exciton formation zone or by shortening triplet exciton lifetime. The introduction of double EMLs[14-19] can broaden the exciton formation zone. But the exciton generation region in double-EML PHOLEDs is still relatively narrow due to the used hosts only featuring either hole or electron transport.[20, 21] Mixed host (MH) structure,[20-26] *i.e.*, the uniform or graded mixture of a hole and an electron transporting material as EML host, is able to provide a broader exciton formation zone and thus leads to a further improvement in efficiency roll-off.[20] However, the doping ratio of the two host materials should be tuned finely to realize the balance of hole and electron transport property. This will inevitably result in the complexity and poor repeatability in device preparation and thus limit the application

of MH structure. The efficiency roll-off behavior can also be improved by multiple quantum well (MQW) structure in the nondoped PHOLEDs.[27] But such structure introduces the complex heterojunctions in the EML to result in high driving voltage and limit device reliability. Because the accumulated charges in heterojunction interfaces are prone to form chemically unstable cationic species which would accelerate the formation of non-radiative trap centers and thus device degradation.[28, 29] Zheng *et al.* developed a fluorescence-interlayer-phosphorescence emission layer structure (FIP EML) to solve the efficiency roll-off issue effectively.[30] But this strategy didn't offer high device efficiency due to the utilization of fluorescent dopant. Recently, Ji *et al.* reported the reduced efficiency roll-off in PHOLEDs using surface plasmon resonance of Au nanoparticles to shorten the triplet exciton lifetime and thus reduce the exciton density.[31] However, the introduction of Au nanoparticles would not only increase the cost but also induce the complexity in device fabrication, which is incompatibility with industrial applications. Hence, it is still essential to explore efficient, economical and simple strategies for reducing efficiency roll-off in PHOLEDs.

In this paper, we demonstrated a PHOLED with both high luminescent efficiency and low efficiency roll-off, in which two ultrathin emission layers [possessing the same host CBP and phosphorescent dopant $Ir(ppy)_3$, but one with high doping ratio and the other with low doping ratio] alternating with each other to form a stack are employed as EML. In our proposed structure, the triplet excitons generated in the high doping regions are able to diffuse more quickly to the neighboring low doping regions compared with the traditional PHOLEDs with uniformly doped host, and therefore triplet exciton quenching is effectively suppressed and then high luminescent efficiency and low efficiency roll-off [peak current efficiency (CE) = 48.8 cd/A, peak external quantum efficiency (EQE) = 19.6%] and low efficiency roll-off (only a less than 25.1% drop in CE and 25.5% drop in EQE when the luminance increases from 1000 cd/m^2 to 100000 cd/m^2) are achieved. Compared with the existing works,[14-26] our proposed has the advantages of easy fabrication, economical, and avoiding interface charge accumulation due to heterojunction-free in EML, which is expected to increase device lifetime as well.[32, 33] Therefore, the stacked EML structure can be used as an effective strategy to develop high efficient and concurrently low efficiency roll-off PHOLEDs.

2. Experimental

The proposed PHOLED has the structure of ITO/MoO_3 (1 nm)/CBP:15 wt% MoO_3 (30 nm)/CBP (10 nm)/[CBP:4 wt% $Ir(ppy)_3$ (5 nm)/CBP:8 wt% $Ir(ppy)_3$ (5 nm)]$_N$/Bphen (40 nm)/LiF (1 nm)/Al (150 nm), where CBP [4, 4'-bis (carbazol-9-yl)-biphenyl] is used as the host of EML and hole-transport-layer (HTL), $Ir(ppy)_3$ [tris(2-phenylpyridine) iridium(III)] as phosphorescent dopant, Bphen [4, 7-Diphenyl-1, 10-Phenanthroline] as hole blocking layer (HBL) and electron transporting layer (ETL), MoO_3 in CBP:MoO_3 as p-dopant and pure MoO_3 with 1 nm-thickness as hole injection layer (HIL), respectively. Besides, the nondoped CBP with 10 nm-thickness is employed to prevent the diffusion of p-dopant MoO_3 from HTL into EML. A key feature of such a PHOLED is two ultrathin emissive layers of CBP:4 wt% $Ir(ppy)_3$ (5 nm) and CBP:8 wt% $Ir(ppy)_3$ (5 nm) alternating with each other to form a periodic stack as EML. There N is equal to 3, representing the number of [CBP:4 wt% $Ir(ppy)_3$ (5 nm)/CBP:8 wt% $Ir(ppy)_3$ (5 nm)] cells. Additionally, there exists only single-heterojunction at EML/ETL interface in the whole device and thus the injection carriers face no abrupt barriers from electrode to EML, as shown in Fig. 1(a).

For comparison, the reference devices B and C were also constructed, as shown in Figure 1(b) and (c), where the entire EML is uniformly doped by the phosphor $Ir(ppy)_3$ with the concentration of 4 wt% in device B and 8 wt% in device C. Fig. 1 also shows the energy level structures of all devices, where the lowest unoccupied molecular orbital (LUMO) and the highest occupied molecular orbital (HOMO) are extracted from Ref. [11, 34]. In addition, the doping concentrations and layer thickness are also displayed in Fig. 1. The doping concentrations are given in weight percentage (wt%).

All the PHOLEDs were fabricated on the pre-cleaned glass substrates coated by indium tin oxide (ITO) with a sheet resistance of 10 Ω/sq. All organic layers and cathode were in turn deposited by thermal evaporation in high vacuum system (base pressure < 5×10^{-4} Pa). The deposited layer thickness and the growth rate were monitored by quartz crystal monitor calibrated by spectroscopic ellipsometry to ensure accuracy. The evaporating rates were kept at 0.1 nm/s for the organic materials, 0.01 nm/s for MoO_3 and LiF as well as 0.5 nm/s for Al. The doped layers were performed by co-evaporating host and dopant loaded in the separate heating sources. All devices have an emitting area of 3×3 mm^2. To eliminate possible run-to-run difference, all devices were fabricated under identical experimental conditions and each device was reproduced for multiple times. The electroluminescent (EL) spectra and luminance-current-voltage (L-C-V) characteristics of devices were measured using SpectraScan PR 655 and KEITHLEY 2400. All measurements were carried out at room temperature under ambient conditions.

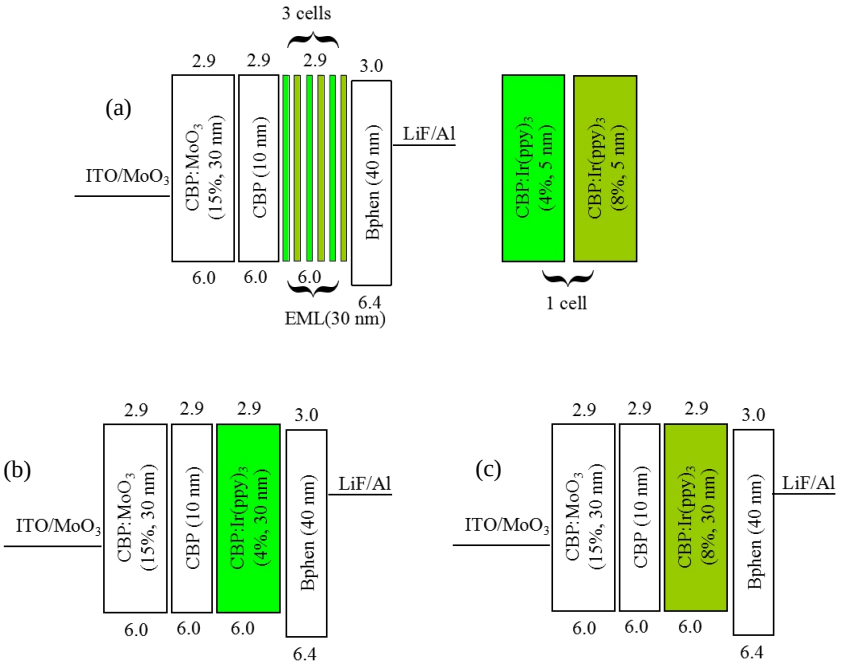

Fig. 1. The structure diagrams of devices A (a), B (b) and C (c) along with their corresponding energy levels.

3. Results and discussion

Fig. 2 shows the CE, EQE and PE versus luminance characteristics of devices A-C. The details of the performances of all devices are summarized in Table 1. It is observed that the efficiency characteristics of device A are dramatically optimal among the three devices. Compared with device B, device A exhibits a peak CE of 48.8 cd/A with the enhancement factor of 50.2%, a

peak EQE of 19.6% with the enhancement factor of 49.6%, and a peak PE of 30.1 lm/W with the enhancement factor of 57.6%. What's more, CE, EQE and PE values of device A keep at a significantly higher level over the observed luminance range. Compared with device C, although the peak efficiencies of device A are not higher, its efficiency roll-off is greatly improved. In details, as the luminance increases from 1000 cd/m^2 to 100000 cd/m^2, a less than 25.1% drop in CE, 25.5% drop in EQE and 54.5% drop in PE are found in device A, while more than 36.5% roll-off in CE, 36.4% roll-off in EQE and 62.3% roll-off in PE are observed in device C. It is concluded that device A combines the merits of device B and C to offer concurrently high efficiency and low efficiency roll-off.

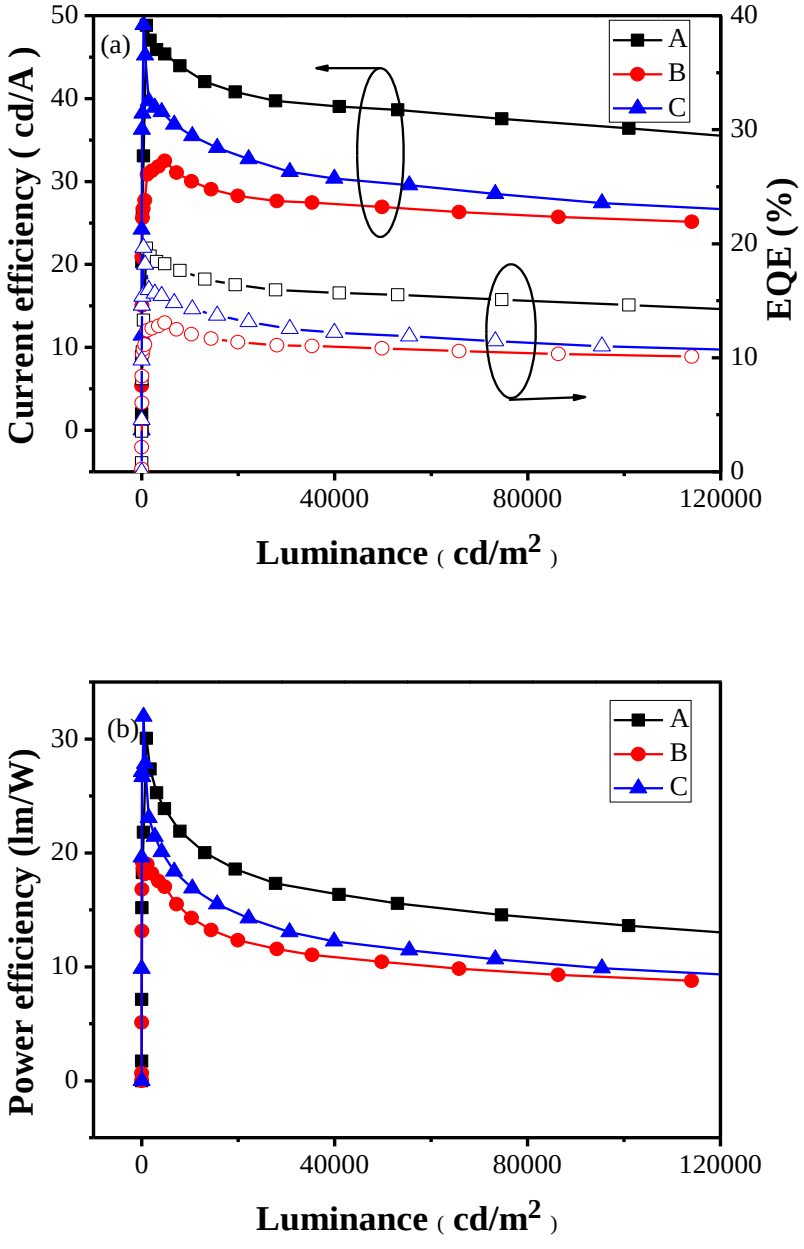

Fig. 2. CE, EQE (a) and PE (b) versus luminance characteristics of devices A-C.

Table 1. The efficiency parameters of devices A, B and C.

Device	CE (cd/A)				EQE(%)				PE(lm/W)			
	Max.	@1000 cd/m^2	@10000 cd/m^2	@100000 cd/m^2	Max.	@1000 cd/m^2	@10000 cd/m^2	@100000 cd/m^2	Max.	@1000 cd/m^2	@10000 cd/m^2	@100000 cd/m^2
A	48.8	48.7	43.2	36.5	19.6	19.6	17.4	14.6	30.1	29.9	21.1	13.6
B	32.5	29.9	30.1	25.4	13.1	12.0	12.1	10.2	19.1	18.7	14.4	9.0
C	48.9	43.0	35.7	27.3	19.6	17.3	14.3	11.0	32.0	26.0	17.1	9.8

To elucidate the mechanism of improved performance in device A, we first probe the reasons of low efficiency in device B and serious efficiency roll-off in device C. The rather low efficiency in device B originates from the low doping ratio of phosphor $Ir(ppy)_3$. The limited doping ratio of $Ir(ppy)_3$ leads to low population of $Ir(ppy)_3$ triplet excions and thus weak $Ir(ppy)_3$ emitting. But device B exhibits a very low efficiency roll-off over the whole observed range, as shown in Fig. 2 (see red circle symbol line). This tells us that a straightforward method of improving efficiency roll-off is to avoid high local exciton density in EML. To illuminate the serious efficiency roll-off in device C, the exciton recombination zone in device C was investigated comprehensively by red phosphor bis(1-phenyl-isoquinoline) (acetylacetonato) iridium(III) [$Ir(piq)_2(acac)$] as a probe. $Ir(piq)_2(acac)$ ultrathin layer with thickness of 1 nm was inserted into three different positions of device C. The three positions are denoted as P1, P2, and P3 [see inset of Fig. 3(a)], which are away from EML/ETL interfaces by 0, 10, and 20 nm, and the corresponding devices are referred to as C^{P1}, C^{P2} and C^{P3} respectively. The normalized EL spectra of them at 4.3 V are displayed in Fig. 3. The comparison of relative EL intensity of the red emission from $Ir(piq)_2(acac)$ and the green emission from $Ir(ppy)_3$ can be used to detect exciton distribution. It can be seen from Fig. 3 that as $Ir(piq)_2(acac)$ probe moves gradually from P1 to P3, red emission became weaker rapidly. The peak ratio of red-to-green emission in device C^{P1} to C^{P3} is 12.85, 4.00 and 0.74 respectively. These results indicate that the main exciton formation zone is located near the interface of EML/ETL with the scale of about 10 nm and then the exciton density decreases fast from P2 to P3 position. A large amount of excitons highly gather in a narrow region to induce an inferior TTA. Besides, due to the more hole transporting property of CBP and the blocking hole role of Bphen, surplus holes could be accumulated at EML/ETL interface and consequently result in TPA. The TTA and TPA give rise to the serious efficiency roll-off in device C.

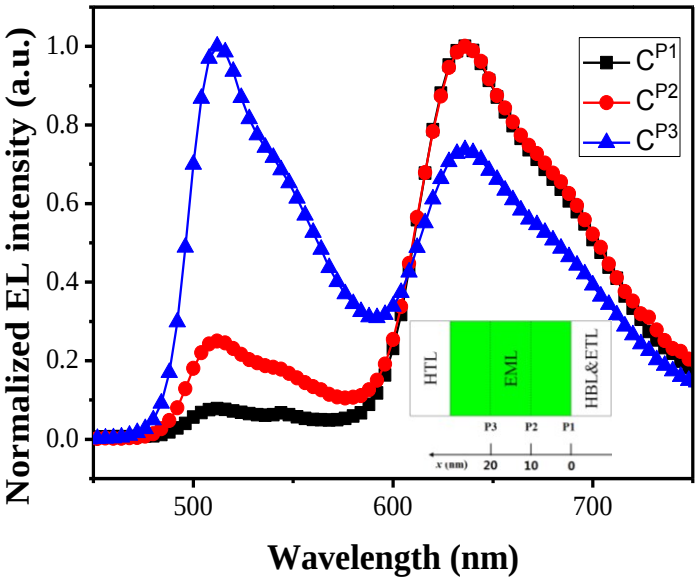

Fig. 3. Normalized EL spectra of devices C^{P1}, C^{P2} and C^{P3} at 4.3 V. Inset: the schematic diagram of the positions of $Ir(piq)_2(acac)$ probe in EML.

Next, we investigate the triplet exciton distribution in device A. For this purpose, additional devices A^{P4} and A^{P5} are designed, in which an ultrathin layer of $Ir(piq)_2(acac)$ (1 nm) is inserted into EML of device A at the position away from EML/ETL interfaces by 3 and 12 nm [see inset of Fig.4(a)], respectively. Similarly, reference devices C^{P4} and C^{P5} were also constructed for comparison, in which $Ir(piq)_2(acac)$ probe is inserted into EML of device C at the similar positions away from EML/ETL interfaces as devices A^{P4} and A^{P5}. Fig. 4(a) depicts the normalized EL spectra of them at 5 V. One can see that green emission from $Ir(ppy)_3$ in device A^{P4} is distinctly stronger than that in device C^{P4} [solid symbol in Fig. 4(a)]. The peak ratio of red-to-green emission decreases from 4.40 in device C^{P4} to 1.62 in device A^{P4}, indicating the triplet exciton density is relatively lower at 3 nm position away from the interface of EML/ETL in device A than in device C. Similar results are also observed in device A^{P5} and C^{P5} [open symbol in Fig. 4(a)]. In addition, when comparing the evolution of normalized EL spectra of device A^{P4} and C^{P4} with driving-voltage increase, see Fig. 4(b) and (c), one can find that the exciton recombination zone shifts faster towards anode side in device A^{P4} than in device C^{P4}, leading to the red emission weaken faster. One possible reason is that the generated triplet exitons are diffused more quickly to neighboring region by the stacked EML structure. Another possible reason is the stacked structure facilitating electron transport and hence making the triplet exiton formation zone shifts towards anode side. In order to identify the role of the stacked EML, two single-electron devices A_1 and C_1 with structures of ITO/Bphen (20 nm)/EML (60 nm)/Bphen (20 nm)/LiF (1 nm)/Al (150 nm) are designed. In device A_1, EML has the stacked structure of [CBP:4 wt% $Ir(ppy)_3$ (5 nm)/CBP:8 wt% $Ir(ppy)_3$ (5 nm)]$_6$, while in device C_1, EML has uniform doping structure of CBP:8 wt% $Ir(ppy)_3$ (60 nm). *J-V* curves of devices A_1 and C_1 are shown in Fig. 5. It can be seen that the electronic transport characteristics of devices A_1 and C_1 are almost the same. This implies that the stacked EML has little effect on the electron transport mobility, which is consistent with *J-V* characteristic of devices A and C (see inset of Fig. 5). Therefore, it is concluded that lower triplet exciton density near the interface of EML/ETL in device A originates more likely from quick exciton diffusion from high doping region to low doping region. Based on the fact that the

exciton recombination zone moves toward the anode side with driving-voltage increase, the periodic stack EML structure is necessary for dispersing the high density triplet exitons at different voltage, and hence achieving high efficiency at high current densities, that is, the reduced efficiency roll-off.

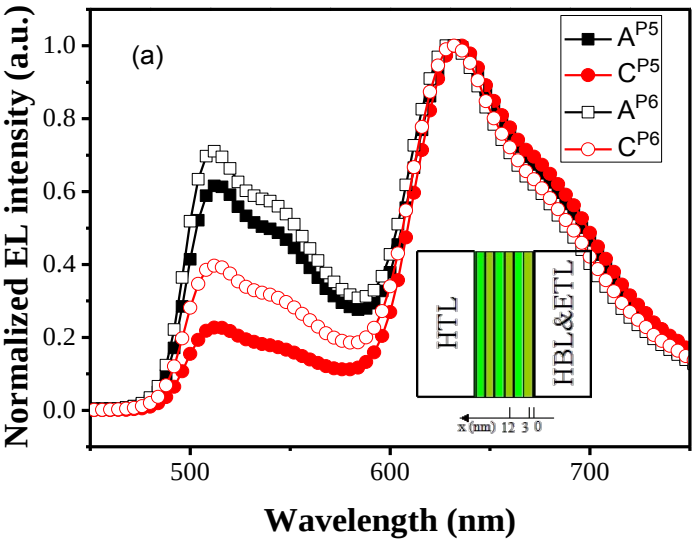

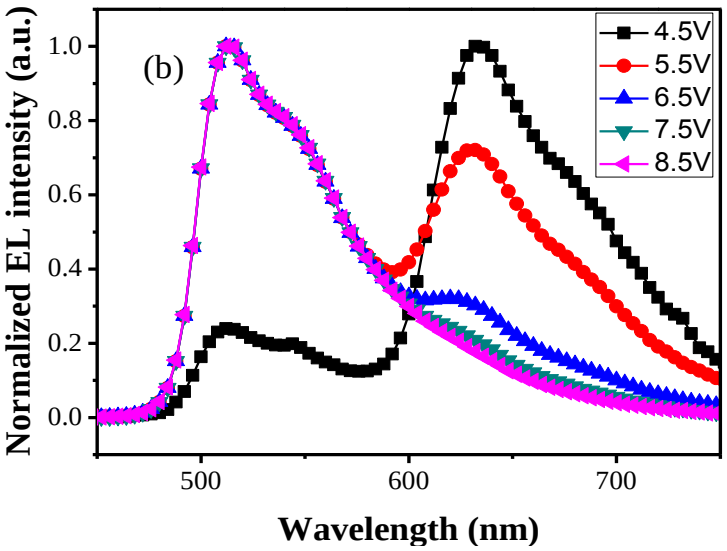

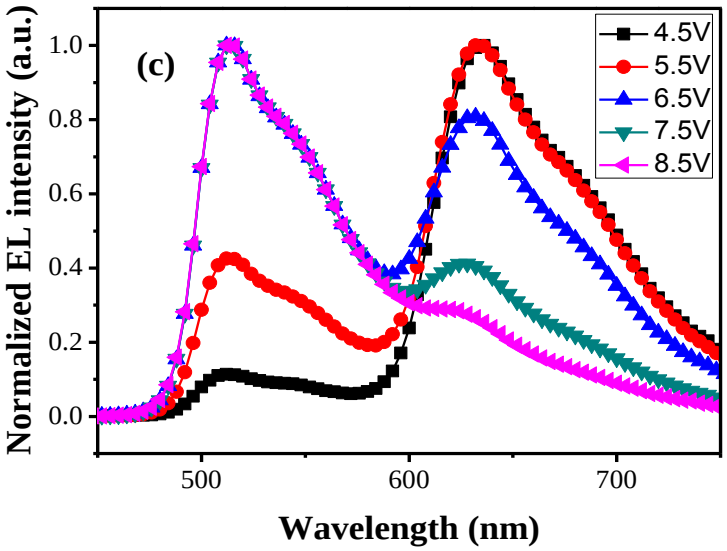

Fig. 4. (a) Normalized EL spectra of devices A^{P4}, A^{P5}, C^{P4} and C^{P5} at 5 V; (b) Normalized EL spectra of device A^{P4} at different voltages; and (c) Normalized EL spectra of device C^{P4} at different voltages. Inset of (a): the schematic diagram of the positions of $Ir(piq)_2(acac)$ probe in EML.

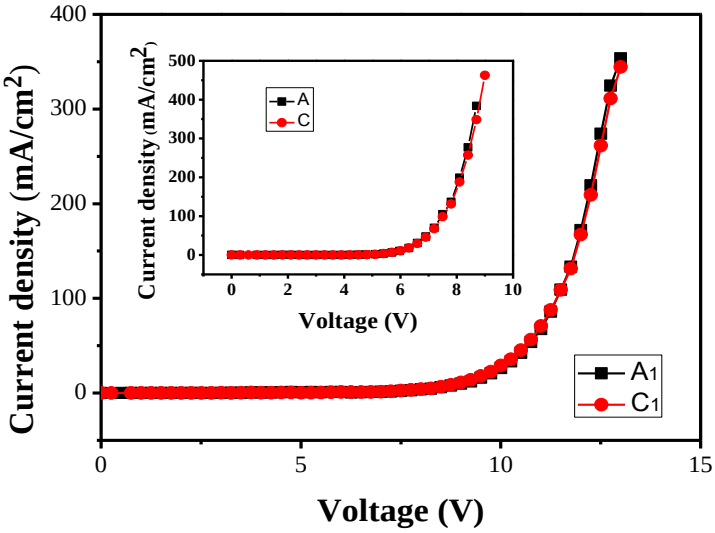

Fig. 5. J-V curves of single-electron devices A_1 and C_1. Inset: J-V curves of devices A and C.

In order to further confirm the deduction that the improved properties of device A are attributed to greatly weakened triplet exciton quenching due to the very effective triplet exciton diffusion by such a stack emissive structure, we design device D, of which except its EML has a three-cell stacked structure $[CBP/CBP:8\ wt\%\ Ir(ppy)_3]_3$, other function layers are completely same as that of device A. In a emissive cell of device D, the concentration of $Ir(ppy)_3$ decreases to zero in one ultrathin layer and maintains at 8 wt% in the other ultrathin layer for achieving more large concentration gradient of $Ir(ppy)_3$ in the EML. Similarly, 1 nm-thick $Ir(piq)_2(acac)$ is also inserted in 3 nm position away from EML/ETL interface in device D to form device D^{P4}. The normalized EL spectra of devices A^{P4} and D^{P4} at 4.5 V are displayed in Fig. 6. One can observe that the peak ratio of red-to-green emission in device D^{P4} is obviously smaller than that in A^{P4}.

This means that the larger concentration gradient of $Ir(ppy)_3$ is more favorable for diffusion of triplet excitons. Of course, device D is not a well-behaved emitting diode due to insufficient amount of $Ir(ppy)_3$ (not shown here).

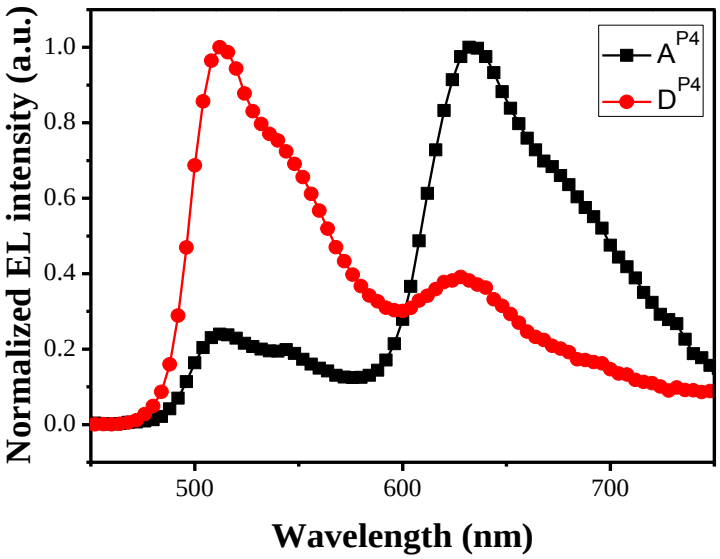

Fig. 6. Normalized EL spectra of devices A^{P4} and D^{P4} at 4.5 V.

To sum up, compared with uniform doping structure, the stack EML structure in device A arises the periodic concentration gradient of $Ir(ppy)_3$ and then facilitates quick exciton diffusion from high doping region to low doping region, as shown in Fig. 7, *i.e.* our proposed could make the triplet exciton more uniformly distribute in device A than in traditional device C, accordingly avoid local high triplet exciton density and reduce the triplet exciton quenching, contributing to the improved efficiency roll-off in device A.

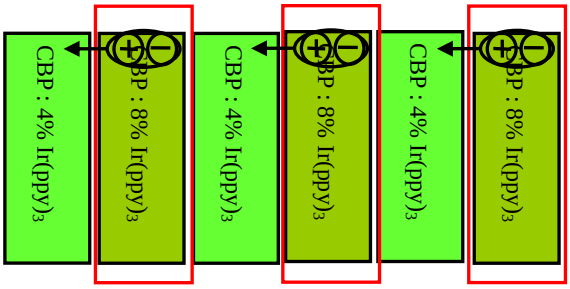

Fig. 7. Model of triplet excitons diffusion in device A

4. Conclusions

We proposed a PHOLED with a stack structure of [CBP:4 wt%$Ir(ppy)_3$ (5 nm)/CBP:8 wt%$Ir(ppy)_3$(5 nm)]$_3$ as EML. Such a structure makes the triplet excitons generated in the high doping regions could diffuse more quickly to the neighboring low doping regions compared with the traditional PHOLEDs with uniformly doping. Therefore the triplet exciton accumulation is effectively reduced and the triplet exciton quenching is greatly weakened and thus high efficiency and low efficiency roll-off are achieved. The current efficiency is kept at a level of ca. 48.8 cd/A and EQE at a level of ca. 19.6% until 1000 cd/m^2. As the luminance increases from 1000 cd/m^2 to 100000 cd/m^2, there exists only about 25.1% drop in current efficiency and 25.5% drop in EQE. Such a stack structure is expected to apply the application not only in PHOLEDs but also in other organic electronic devices for facilitating exciton diffusion.

Acknowledgements

This research work was financially supported by National Natural Scientific Foundation of China (61274056, 61571317, 11204205, 61475109, 11204202, 61308093), Key Laboratory Foundation of Advanced Display and System Applications of Ministry of Education in Shanghai University, special/Youth Foundation of Taiyuan University of Technology (No. 1205-04020102), International Science & Technology Cooperation Program of China (2012DFR50460), Outstanding Young Scholars of Shanxi Province, the New Teachers' Fund for Doctor Stations (20121402120017, 20131402120020), Hong Kong Scholar Plan (XJ2013002), Doctoral Program of Higher Education Research Fund (20121402120017), and the Top Young Academic Leaders of Higher Learning Institutions of Shanxi.

References

1. S. Reineke, F. Lindner, G. Schwartz, N. Seidler, K. Walzer, B. Lüssem and K. Leo, *Nature*, 2009, **459**, 234.
2. Y. Sun, N. C. Giebink, H. Kanno, B. Ma, M. E. Thompson and S. R. Forrest, *Nature*, 2006, **440**, 908.
3. C. Adachi, M. A. Baldo, M. E. Thompson and S. R. Forrest, *J. Appl. phys.*, 2001, **90**, 5048.
4. Y. Miao, X. Du, H. Wang, H. Liu, H. Jia, B. Xu, Y. Hao, X. Liu, W. Li and W. Huang, *RSC Adv.*, 2015, **5**, 4261.
5. W. Ji, J. Wang, Q. Zeng, Z. Su and Z. Sun, *RSC Adv.*, 2013, **3**, 14616.
6. M. A. Baldo, D. F. O'Brien, Y. You, A. Shoustikov, S. Sibley, M. E. Thompson and S. R. Forrest, *Nature*, 1998, **395**, 151.
7. Y. J. Doh, J. S. Park, W. S. Jeon, R. Pode and J. H. Kwon, *Org. Electron.*, 2012, **13**, 586.
8. Q. Yang, Y. Hao, Z. Wang, Y. Li, H. Wang and B. Xu, *Synth. Met.*, 2012, **162**, 398.
9. M. A. Baldo, C. Adachi and S. R. Forrest, *Phys. Rev. B: Condens. Matter*, 2000, **62**, 10967.
10. S. Reineke, K. Walzer and K. Leo, *Phys. Rev. B: Condens. Matter*, 2007, **75**, 125328.
11. T. L. Li, W. L. Li, B. Chu, Z. S. Su, Y. R. Chen, L. L. Han, D. Y. Zhang, X. Li, F. X. Zang and T. C. Sum, *J. Phys. D: Appl. Phys.*, 2009, **42**, 065103.
12. Y. Li, Y. Hao, Z. Yan, H. Liu, H. Wang and B. Xu, *Synth. Met.*, 2013, **164**, 12.
13. F. X. Zang, T. C. Sum, A. C. H. Huan, T. L. Li, W. L. Li and F. Zhu, *Appl. phys. lett.*, 2008, **93**, 023309.
14. G. He, M. Pfeiffer, K. Leo, M. Hofmann, J. Birnstock, R. Pudzich and J. Salbeck, *Appl. phys. lett.*, 2004, **85**, 3911.
15. J.-W. Kang, S.-H. Lee, H.-D. Park, W.-I. Jeong, K.-M. Yoo, Y.-S. Park and J.-J. Kim, *Appl. phys. lett.*, 2007, **90**, 223508.
16. J. Lee, J.-I. Lee and H. Y. Chu, *Synth. Met.*, 2009, **159**, 1460.
17. Z. Ma, S. Zhou, S. Hu and J. Yu, *J. Lumin.*, 2014, **154**, 376.
18. S.-J. Su, E. Gonmori, H. Sasabe and J. Kido, *Adv. Mater.*, 2008, **20**, 4189.
19. J.-H. Lee, C.-L. Huang, C.-H. Hsiao, M.-K. Leung, C.-C. Yang and C.-C. Chao, *Appl. phys. lett.*, 2009, **94**, 223301.
20. N. C. Erickson and R. J. Holmes, *Adv. Funct. Mater.*, 2013, **23**, 5190.
21. N. C. Erickson and R. J. Holmes, *Adv. Funct. Mater.*, 2014, **24**, 6074.
22. N. Chopra, J. S. Swensen, E. Polikarpov, L. Cosimbescu, F. So and A. B. Padmaperuma, *Appl.*

phys. lett., 2010, **97**, 033304.

23. S. H. Kim, J. Jang, K. S. Yook and J. Y. Lee, *Appl. phys. lett.*, 2008, **92**, 023513.
24. J. Lee, J.-I. Lee, J. Y. Lee and H. Y. Chu, Org. Electron., 2009, **10**, 1529.
25. J. Lee, J.-I. Lee, J. Y. Lee and H. Y. Chu, *Appl. phys. lett.*, 2009, **94**, 193305.
26. N. C. Erickson and R. J. Holmes, *Appl. phys. lett.*, 2010, **97**, 083308.
27. S. Liu, B. Li, L. Zhang, H. Song and H. Jiang, *Appl. phys. lett.*, 2010, **97**, 083304.
28. D. Y. Kondakov, J. R. Sandifer, C. W. Tang and R. H. Young, *J. Appl. phys.*, 2003, **93**, 1108.
29. D. Y. Kondakov and R. H. Young, *J. Appl. phys.*, 2010, **108**, 074513.
30. T. Zheng, W. C. H. Choy, C. L. Ho and W. Y. Wong, *Appl. phys. lett.*, 2009, **95**, 133304
31. W. Ji, L. Zhang and W. Xie, *Opt. lett.*, 2012, **37**, 2019.
32. J.-R. Koo, S. J. Lee, G. W. Hyung, D. W. Im, H. S. Yu, J.-H. Park, K. H. Lee, S. S. Yoon, W. Y. Kim and Y. K. Kim, *AIP Adv.*, 2012, **2**, 012117.
33. Y. Li, Y. Hao, W. Li, S. Yuan, H. Liu, Y. Cui, H. Wang, B. Xu and W. Huang, *Opt. Express*, 2013, **21**, 17020.
34. D. Yang, W. Li, B. Chu, D. Zhang, J. Zhu, Z. Su, W. Su, L. Han, D. Bi and Y. Chen, *Appl. phys. lett.*, 2008, **92**, 253309.